Design of *p*-type transparent conductors from inverted band structure: The case of inorganic metal halide perovskites

Peng Zhang,[1,2] Shu Yu,[1] Xiuwen Zhang,[1,*] and Su-Huai Wei[2,†]
[1]*College of Physics and Optoelectronic Engineering, Shenzhen University, Shenzhen, Guangdong 518060, China*
[2]*Beijing Computational Science Research Center, Beijing 100193, China*

(Received 28 January 2019; published 15 May 2019)

Transparent conductors (TCs), which bring two seemingly contraindicated properties, conductivity and transparency, together into one material, enable many critical technologies. Significant successes have been achieved for *n*-type TCs, such as Sn-doped In_2O_3, but developing their *p*-type counterparts has still encountered a big challenge, mainly due to the intrinsic band structure of conventional semiconductors. Here, we propose that a class of wide-gap inorganic metal halide perovskites have great potential as ideal *p*-type TCs, because of their inverted band structure compared to *n*-type TCs, i.e., they have *s*-like wave-function character at the top of the valence band, and *p*-like wave-function character at the lower valence bands and the bottom of the conduction band, which results in significantly improved *p*-type dopability, high hole mobility, and good optical transparency. This insight of designing *p*-type TCs from an inverted band structure opens an avenue for the future design of critical optoelectronic materials.

DOI: 10.1103/PhysRevMaterials.3.055201

I. INTRODUCTION

Transparent conductors (TCs) are essential for many modern optoelectronic devices, such as transparent thin-film transistors, touch-screen sensors, solar cells, flat-panel displays, and light-emitting diodes [1–7]. Currently, all the commercially available TCs are based on *n*-type oxides, such as Sn-doped In_2O_3 and electron-doped ZnO, whereas the fabrication of their *p*-type counterparts has still been a big challenge, which seriously impedes the further exploration of transparent electronics with novel functionalities. The difficulty in achieving *p*-type TCs in oxides (i.e., TCOs) roots mainly from two critical features of their band structures, as schematically illustrated in Fig. 1(a): (i) the valence-band maximum (VBM) of TCOs is usually dominated by the low-lying localized O $2p$ orbitals, which based on the "doping limit rule" will eventually lead to high acceptor formation energies, deep acceptor levels, poor hole mobility, and thus poor *p*-type conductivity [8–11]; (ii) the energy difference between the VBM and lower valence-band (VB) states in TCOs is relatively small, due to the degeneracy of O $2p$ bands, which will trigger the intraband optical absorptions as the materials are heavily doped *p* type, and thus degrade the transparency [12–14]. On the contrary, the conduction- band minimum (CBM) of TCOs is predominately derived from the low-lying delocalized cation *s* orbital, which ensures good *n*-type dopability, high electron mobility, and thus good *n*-type conductivity. Moreover, the large energy separation between the CBM and higher conduction-band (CB) states results in negligibly small intraband absorptions for visible light, which guarantees the transparency when the materials are doped *n* type [15–17].

This characteristic band structure of TCOs implies that it may be a formidable task to make oxides as *p*-type TCs; however, it meanwhile points out an important design strategy for realizing both the *p*-type conductivity and optical transparency in other materials: If one can find materials that have a band structure, where the VBM has a predominate *s* character and the CBM has a *p* character, as illustrated in Fig. 1(b), the good *n*-type conductivity in TCOs can then be transferred into good *p*-type conductivity in these materials. Meanwhile, the large energy separation between the *s*-like VBM and *p*-like lower VB states may be also obtained, which will retain the transparency as the materials are doped *p* type. This characteristic band structure for *p*-type TCs can be viewed as an exact "inverted band structure" of TCOs; nevertheless, the question is whether we can find promising candidates that satisfy this design strategy. Moreover, to be practical *p*-type TCs, additional criteria beside the *p*-type conductivity and transparency should also be satisfied, such as (i) high thermodynamic stability (ii) good defect tolerance ability, and (iii) ease to fabricate.

In principle, for systems with an inverted band structure, the cation *s* orbital should form occupied bands with relatively low energy [see Fig. 1(b)], which can be achieved in compounds containing heavy elements with low valence states, such as Pb^{2+} and Bi^{3+}, because the large relativistic effect pushes down their occupied *s* orbital in energy. In oxides, one example of these systems is the Sn^{2+}-based compounds, such as SnO and K_2SnO_3, which however exhibit either small optical band gaps or poor thermodynamic stability, preventing them from practical applications as *p*-type TCs [7,18,19]. More recently, a new class of inorganic metal halide perovskites (IMHPs) has emerged with superb optoelectronic properties [20–27]. Among them, $CsPbCl_3$ shows a short emission wavelength of ∼410 nm, corresponding to a band gap of ∼3.0 eV, guaranteeing the good transparency for most

*xiuwenzhang@szu.edu.cn
†suhuaiwei@csrc.ac.cn

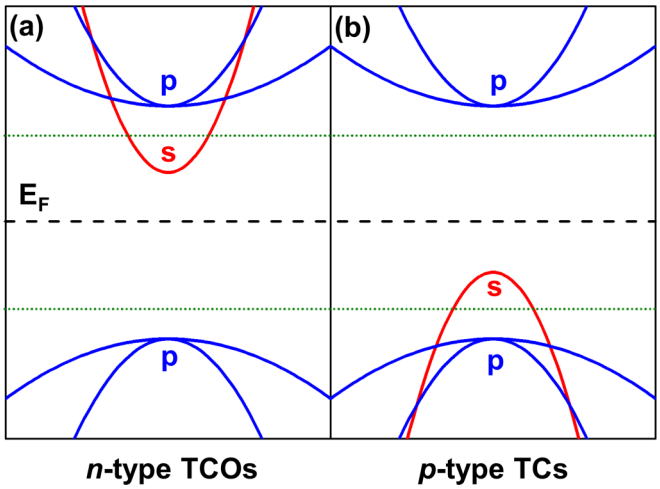

FIG. 1. Schematic illustration of (a) normal band structure for conventional semiconductors, such as In_2O_3, and (b) inverted band structure for *p*-type TCs. The black dashed line indicates the position of Fermi level, while the green dotted lines present the doping-limit energy level.

of the visible light [28]. Moreover, the theoretical calculations [21] have shown that IMHPs have a typical inversed band structure of conventional semiconductors, e.g., their VBM (CBM) is analogous to the CBM (VBM) of GaAs. The wide band gap, combined with this unique band structure, thus suggests that IMHPs can be promising *p*-type TCs. In this paper, based on the first-principles calculations, we systematically study the electronic structure, dielectric function, plasma frequency, optical absorption spectra, and defect property of IMHPs. Based on the examination of both the optical transparency and electrical conductivity, we propose that $CsPbCl_3$, $RbPbCl_3$, and $CsPbBr_3$ could be promising candidates for *p*-type TCs.

II. COMPUTATIONAL METHOD

The first-principles calculations are carried out by using the projector-augmented wave method [29] and Heyd-Scuseria-Ernzerhof (HSE06) hybrid functional [30] within the density-functional theory as implemented in VASP [31]. The wave functions are expanded by using the plane waves up to a kinetic energy cutoff of 400 eV. Brillouin-zone integrations are approximated by using special *k*-point sampling of Monkhorst-Pack scheme with a *k*-point mesh resolution of $2\pi \times 0.03/\text{Å}^{-1}$. The cell lattice vectors and atomic coordinates are fully relaxed until the force on each atom is less than 0.01 eV/Å. For the band-structure calculation, GW method [32] with spin-orbital coupling (GW+SOC) is also employed and compared with the HSE06 results.

For the defect calculations of $CsPbCl_3$, we construct a 320-atom supercell with a single Γ point. For a defect α in the charge state q, its formation energy $[\Delta H_f(\alpha, q)]$ can be calculated by [33,34]

$$\Delta H_f(\alpha, q) = \Delta E(\alpha, q) + \sum n_i \mu_i + qE_F, \quad (1)$$

where $\Delta E(\alpha, q) = E(\alpha, q) - E(\text{host}) + \sum n_i E_i + q\varepsilon_{\text{VBM}}$ (host). Here, $E(\text{host})$ is the total energy of the supercell and $E(\alpha, q)$ is the total energy of the same supercell, but with a defect α. The E_F is referenced to the VBM of the host, μ_i is the chemical potential of constituent element i referenced to elemental solid or gas with energy E_i, n_i is the number of elements, and q is the number of electrons transferred from the supercell to reservoirs in forming the defect cell. It should be mentioned that μ_i is not a free variable, but limited by a series of conditions. First, to avoid the formation of elementary solid, it is required that $\mu_i < 0$. Second, to avoid the formation of the competing secondary phases, such as CsCl, μ_i must satisfy

$$\mu_{\text{Cs}} + \mu_{\text{Cl}} < \Delta H_f(\text{CsCl}), \quad (2)$$

where $\Delta H_f(\text{CsCl})$ is the formation energy of CsCl (cubic structure, space group $Fm\bar{3}m$). Similarly, other possible secondary phases must also be avoided, including $PbCl_2$ (tetragonal structure, space group $P4_2/mnm$), $PbCl_4$ (monoclinic structure, space group $C2/c$), and Cs_2PbCl_6 (cubic structure, space group $Fm3m$). For extrinsic defects, the additional secondary phases, such as NaCl, KCl, and AgCl (cubic structure, space group Fm-$3m$), are also considered. Finally, to make $CsPbCl_3$ stable, it is also required that

$$\mu_{\text{Cs}} + \mu_{\text{Pb}} + 3\mu_{\text{Cl}} = \Delta H_f(\text{CsPbCl}_3). \quad (3)$$

With all of these restrictions considered, the stable chemical potential range for $CsPbCl_3$ can be determined [see Fig. 4(a)]. For the A point (i.e., under Pb-rich condition), μ_{Cs}, μ_{Pb}, μ_{Cl}, μ_{Na}, and μ_{K} are determined to be −2.23, 0.00, −1.99, −1.93, and −2.15 eV, respectively; while for the C point (i.e., under Pb-poor condition), μ_{Cs}, μ_{Pb}, μ_{Cl}, μ_{Na}, and μ_{K} are determined to be −4.25, −3.34, −0.21, −3.71, and −3.95 eV, respectively.

The transition energy level of a defect α between charge states q and q', $\varepsilon_\alpha(q/q')$, with respect to the VBM, is calculated from the formation energies by

$$\varepsilon_\alpha(q/q') = \frac{\Delta E(\alpha, q) - \Delta E(\alpha, q')}{q' - q} - \varepsilon_{\text{VBM}}. \quad (4)$$

III. RESULTS AND DISCUSSION

To guarantee the transparency of *p*-type TCs, several criteria must be satisfied. First of all, the material must have a wide optical band gap (typically >2.5 eV) to ensure that the interband absorptions are negligible, as indicated by T1 in Fig. 2(a). Secondly, besides the interband absorptions, the intraband absorptions within the VB, as indicated by T2 in Fig. 2(a), must also be minimized. Finally, as the materials are doped *p* type, the absorptions and reflections due to the free carries (i.e., plasmonic effect) should be insignificant.

With these basic ideas in mind, we examine the transparency of $CsPbCl_3$, a prototype material of IMHPs. Figure 2(b) shows the calculated band structure of $CsPbCl_3$ with the cubic crystal structure. It is clear to see that the CBM of $CsPbCl_3$ is composed mainly of Pb 6*p* orbitals, while the VBM is constructed by the mixture of Pb 6*s* and Cl 3*p* orbitals, indicating a typical inverted band structure [as

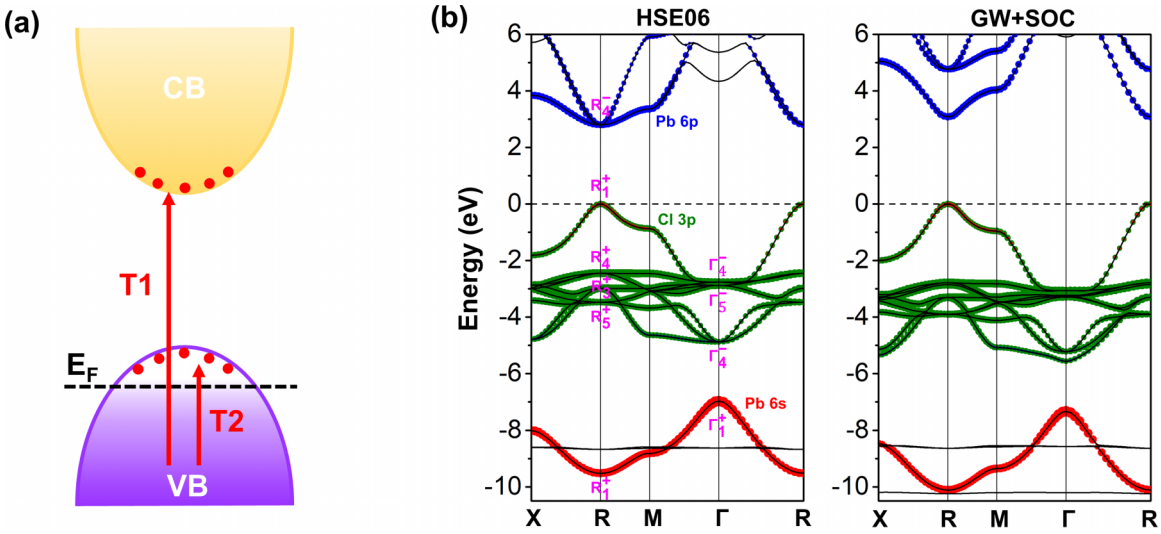

FIG. 2. (a) Interband (T1) and intraband (T2) optical transitions in *p*-type TCs. (b) Band structures of $CsPbCl_3$ calculated by HSE06 and GW+SOC methods.

illustrated in Fig. 1(b)]. The calculated band gap is 2.83 eV, well satisfying the requirement for TCs. We note that this value is slightly smaller than the experimental result for $CsPbCl_3$ nanocrystals (∼3.02 eV) [26], which should be ascribed to the absence of quantum confinement in bulk materials. To evaluate the relativistic effect of Pb, the spin-orbit coupling (SOC) effect is also considered within the GW framework (GW+SOC) [32], as shown in the right panel of Fig. 2(b). Comparing the HSE06 and GW+SOC results, we note that the correct band gap obtained by HSE06 is only a fortuitous result, originating from the accidental cancelation of underestimating the band gap by HSE06 and neglecting SOC at the same time. However, as shown in Fig. 2(b), SOC is actually not important in our calculations, because it influences mainly the CBM, while leaving the VBM almost unchanged. Since we are concerned primarily with the *p*-type doping in $CsPbCl_3$, which is referenced to the VBM, the SOC effect can be safely ignored.

While the wide band gap between CBM and VBM prohibits the interband absorptions of $CsPbCl_3$, the intraband absorptions also need to be checked. This is because, when the materials are doped *p* type and holes are introduced into the VB, the electrons originally occupying the lower VB states can absorb photons and jump into these unoccupied valence states, which would significantly influence the transparency. Fortunately, we find that for $CsPbCl_3$ with the inversion symmetry, the VB states at the R point in the Brillouin zone all possess even parity, as shown in Fig. 2(b). Consequently, the dipole transitions between these VB states are forbidden by symmetry. The dipole-forbidden transitions have been previously found to be important to minimize the interband absorptions in *n*-type In_2O_3 [17] and Cd_2SnO_4 [14]. Here, the similar mechanism would work to minimize the intraband absorptions in *p*-type $CsPbCl_3$. To test this expectation, the optical absorption spectrum of *p*-type doped $CsPbCl_3$ with a hole concentration of $2.8 \times 10^{19}\,\mathrm{cm}^{-3}$ is

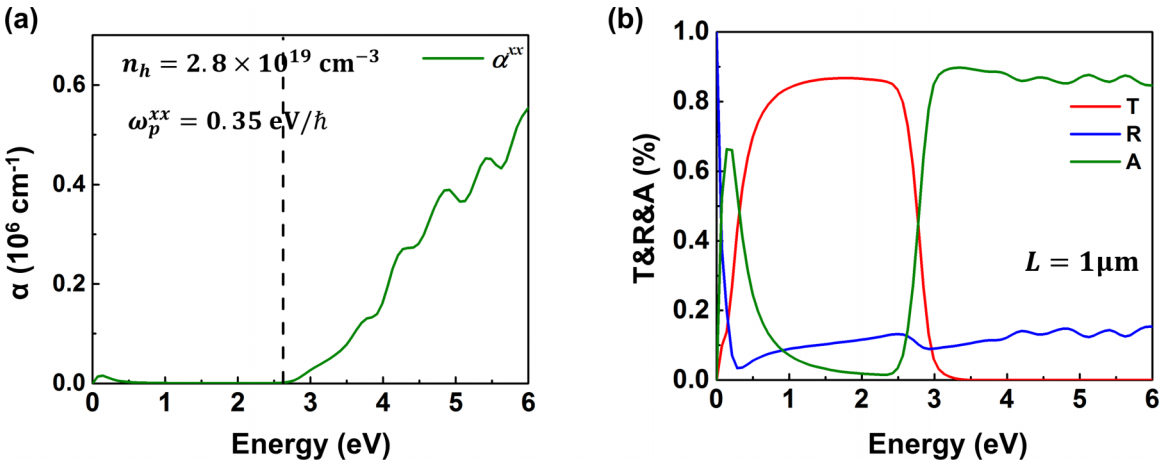

FIG. 3. (a) Calculated absorption coefficient ($\alpha^{xx} = \alpha^{yy} = \alpha^{zz}$) of $CsPbCl_3$. The dashed line shows the energy position of the band gap. (b) Transmission (T), reflection (R), and absorption (A) spectra of a freestanding 1-μm-thick $CsPbCl_3$ film with optically smooth surface. In (a), the hole concentration n_h and plasma frequency $\omega_p^{xx} = \omega_p^{yy} = \omega_p^{zz}$ are also given.

TABLE I. Calculated hole effective mass in $CsPbCl_3$, $RbPbCl_3$, and $CsPbBr_3$.

System	Effective mass of hole (in m_0)
$CsPbCl_3$	0.20
$RbPbCl_3$	0.18
$CsPbBr_3$	0.17

calculated, as shown in Fig. 3(a). The onset of nonplasmonic absorption (the first absorption peak in the infrared range is caused by the plasmonic effect) is found to occur at 2.77 eV, which is slightly smaller than the band gap of intrinsic $CsPbCl_3$, which can be ascribed to the intraband transitions between the top and lower VB states at k points away from R. However, as shown in Fig. 3(a), these intraband transitions are relatively weak and should have insignificant impacts on the transparency of p-type $CsPbCl_3$. For the plasmonic effect of free carriers, we evaluate the plasma frequency ω_p ($\omega_p \sim \sqrt{n_h/m_h^*}$, where n_h is the hole concentration and m_h^* the hole effective mass) from the calculated band structure, and calculate the plasma-induced absorptions and reflections based on the classical Drude model. As shown in Fig. 3(a), the evaluated plasma frequency (0.35 eV/$\hbar$) is low enough to ensure the transparency of p-type $CsPbCl_3$. Figure 3(b) plots the simulated optical transmission, reflection, and absorption spectra for a freestanding 1-μm-thick $CsPbCl_3$ slab with optically smooth surface, which shows that the sample has a very high transmittance (T), low reflectance (R), and low absorption (A) for most of the visible spectral region.

Besides the transparency, another important requirement for p-type TCs is to realize high electrical conductivity ($\sigma \sim n_h e^2 \tau / m_h^*$, where e is the elementary charge and τ is the relaxation time). To achieve this goal, either a small m_h^* or a large n_h is required. For a given material, m_h^* can be easily deduced from the electronic structure, while n_h is closely related to the p-type dopability. The calculated value of m_h^* of $CsPbCl_3$ is ~0.21 m_0 (m_0 is the rest mass of an electron), as given in Table I, which is comparable to the electron effective masses found in n-type TCOs (typically 0.20 ~ 0.35 m_0) and much smaller than that of Cu-based p-type TCOs [7]. This small m_h^* (i.e., large dispersion near VBM) of $CsPbCl_3$ is induced by the hybridization between the delocalized Pb 6s and the Cl 3p orbitals, as shown in Fig. 2(b), which implies a good hole-transport property. Similar band structures have also been found in other IMHPs, such as $CsSnI_3$ that exhibits very high hole mobility of 585 $cm^2\,V^{-1}\,s^{-1}$ at room temperature [35].

To assess the p-type dopability, we calculate the defect properties of $CsPbCl_3$. A series of possible intrinsic defects, including vacancies, antisites, and interstitials, as well as two possible defect complexes and three extrinsic defects (Na_{Pb}, K_{Pb}, and Ag_{Pb}) in the stable chemical potential region are considered, as shown in Fig. 4. The extrinsic dopants Na, K, and Ag are chosen from the groups IA and IB in the Periodic Table, for their closely matching ionic radii (Na^+ : 1.02 Å, K^+ : 1.38 Å, and Ag^+ : 1.15 Å [36]) with Pb^{2+} (1.19 Å) on the octahedral site of $CsPbCl_3$. The defect calculations indicate that $CsPbCl_3$ synthesized under the Pb-poor condition will possess very good p-type dopability, due to the following reasons: (i) the formation energies of acceptor defects (e.g., the intrinsic V_{Cs}^- and V_{Pb}^{2-}, as well as extrinsic K_{Pb}^-, Na_{Pb}^-, and Ag_{Pb}^-) under the Pb-poor condition are relatively low, which ensures that a significant amount of acceptors can be doped into the material. It is surprising to see that the calculated formation energy of Ag_{Pb}^- with the Fermi level at the VBM is only 0.16 eV, which is one order of magnitude lower than that of Sn_{In} in Sn-doped In_2O_3 [37]. Based on this calculated formation energy, we estimate that the defect concentration

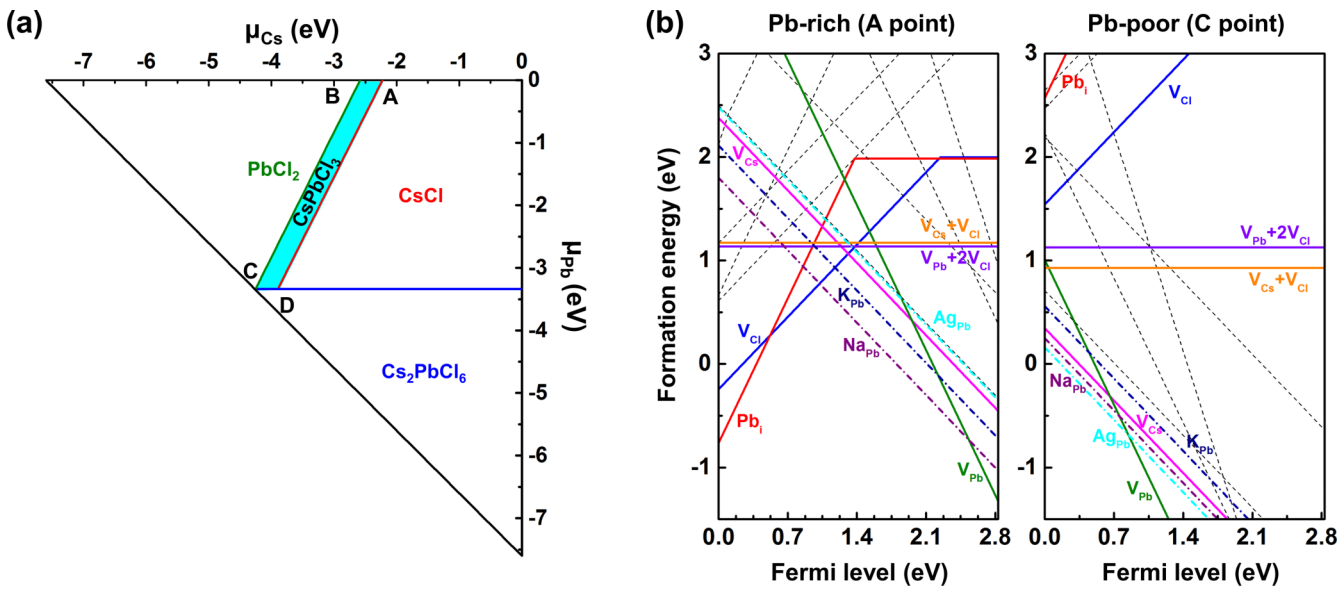

FIG. 4. (a) Stable chemical potential region for the representative ABX_3 ($CsPbCl_3$) showing the potential competing phases (AX,BX_2, A_2BX_6, and B on the border of the stability region). (b) Calculated formation energies for various intrinsic defects, two defect complexes, and three extrinsic defects (K_{Pb}, Na_{Pb}, and Ag_{Pb}) in $CsPbCl_3$, under both the Pb-rich and Pb-poor conditions.

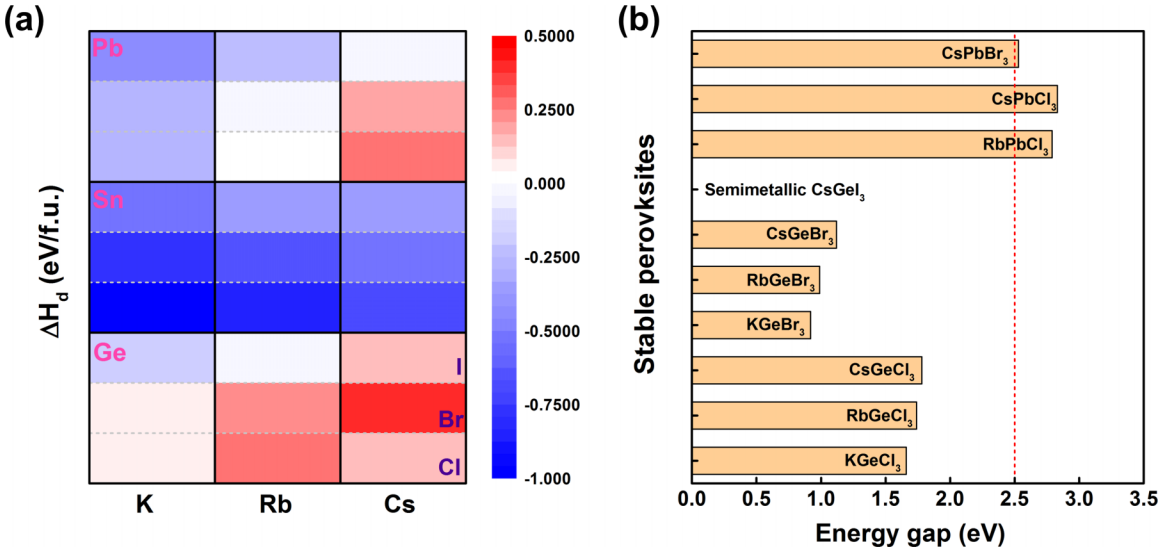

FIG. 5. (a) Decomposition energies (ΔH_d) of 27 IMHPs. (b) Band gaps of 10 stable IMHPs, calculated with GW+SOC method.

of Ag_{Pb}^{-} can be as high as $5.2 \times 10^{19}\,cm^{-3}$ at a relatively low synthesis temperature of approximately 400 K [27]. (ii) All of the above acceptors yield shallow defect levels, which is required to provide a high carrier density, as well as to avoid the electron-hole recombination and coloring of the material. These results are consistent with the fact that, due to the strong coupling between the cation s and anion p orbitals, the VBM of $CsPbCl_3$ is pushed up significantly in energy [8,9].

With this basic understanding on the prototype $CsPbCl_3$, other IMHPs are also inspected. We have considered the thermodynamic stability and band gaps for 27 kinds of IMHPs, with a general formula ABX_3, where $A = $ Cs, Rb, $B = $ Ge, Sn, Pb, and $X = $ Cl, Br, I, as shown in Fig. 5. Among these 27 IMHPs, only 10 of them show thermodynamic stability. For Pb-based IMHPs, we find that only $RbPbCl_3$, $CsPbCl_3$, and $CsPbBr_3$ are stable, while all other compounds tend to decompose. For Sn-based IMHPs, on the other hand, all the compounds are found to be unstable, which is consistent with the experimental observations that $CsSnI_3$ is likely to be oxidized into Cs_2SnI_6, when exposed to moist air or under raised temperatures [38], while for Ge-based IMHPs, we find that most of the compounds are stable, except for $KGeI_3$ and $RbGeI_3$. Moreover, the GW+SOC calculations indicate that, among the ten stable IMHPs, only three candidates have band gaps that satisfy the TCs' requirement (>2.5 eV), while all the others are opaque in the visible spectral range. The largest band gap is found for $CsPbCl_3$, while the band gaps of $RbPbCl_3$ and $CsPbBr_3$ are calculated to be 2.78 and 2.52 eV, respectively. Furthermore, we find that $RbPbCl_3$ and $CsPbBr_3$ can possess even smaller hole effective masses of 0.18 and $0.17m_0$ than $CsPbCl_3$, as shown in Table I, which implies high hole mobility in both of these materials.

IV. CONCLUSION

In summary, we propose an "inverted band-structure" design strategy for realizing p-type TCs, analogous to their n-type counterparts (e.g., In_2O_3). This conceptual design strategy guides us to the finding of a class of p-type TCs based on IMHPs. Our calculations indicate that IMHPs can exhibit wide band gaps of >2.5 eV, which ensures weak interband absorptions in the visible spectral region. Moreover, we find that the intraband absorptions in IMHPs are also very weak, because the symmetry of the perovskite structure forbids the dipole transitions between the VBM and lower VB states. Unlike all the previously proposed p-type TCs, the inverted band structure of IMHPs not only leads to a high VBM energy, but also highly dispersed VBM states, ensuring both good p-type dopability and high hole mobility. The defect calculations for the prototype $CsPbCl_3$ indicate that IMHPs can be easily doped p type at the Pb-poor condition. This characteristic inverted band structure of IMHPs (e.g., $CsPbCl_3$, $RbPbCl_3$, and $CsPbBr_3$) could be found in a wide range of materials which contains cations with filled s^2 lone-pair orbitals and empty p^6 orbitals (e.g., Te^{4+}, Bi^{3+}, Sb^{3+}, and Pb^{2+}). Our study therefore provides an approach to realize high-performance p-type TCs for future applications.

ACKNOWLEDGMENTS

This work is supported by the Science Challenge Project, under Grant No. TZ2016003, the National Key R&D Program of China (Grant No. 2016YFB0700700), and National Natural Science Foundation of China (Grants No. 51672023, No. 11634003, No. U1530401, No. 61827815, and No. 11774239). We also acknowledge the computational support from the Beijing Computational Science Research Center (CSRC).

[1] K. Chopra, S. Major, and D. Pandya, Thin Solid Films **102**, 1 (1983).

[2] K. Nomura, H. Ohta, K. Ueda, T. Kamiya, M. Hirano, and H. Hosono, Science **300**, 1269 (2003).

[3] J. F. Wager, Science **300**, 1245 (2003).
[4] K. Nomura, H. Ohta, A. Takagi, T. Kamiya, M. Hirano, and H. Hosono, Nature (London) **432**, 488 (2004).
[5] T. Minami, Semicond. Sci. Technol. **20**, S35 (2005).
[6] C. G. Granqvist, Sol. Energy Mater. Sol. Cells **91**, 1529 (2007).
[7] K. H. Zhang, K. Xi, M. G. Blamire, and R. G. Egdell, J. Phys.: Condens. Matter **28**, 383002 (2016).
[8] S. B. Zhang, S.-H. Wei, and A. Zunger, J. Appl. Phys. **83**, 3192 (1998).
[9] S. B. Zhang, S.-H. Wei, and A. Zunger, Phys. Rev. Lett. **84**, 1232 (2000).
[10] S. B. Zhang, S.-H. Wei, and A. Zunger, Phys. Rev. B **63**, 075205 (2001).
[11] C. H. Park, S. B. Zhang, and S.-H. Wei, Phys. Rev. B **66**, 073202 (2002).
[12] H. Kawazoe, M. Yasukawa, H. Hyodo, and M. Kurita, Nature (London) **389**, 939 (1997).
[13] A. Kudo, H. Yanagi, H. Hosono, and H. Kawazoe, Appl. Phys. Lett. **73**, 220 (1998).
[14] X. Nie, S.-H. Wei, and S. B. Zhang, Phys. Rev. Lett. **88**, 066405 (2002).
[15] V.-A. Ha, D. Waroquiers, G.-M. Rignanese, and G. Hautier, Appl. Phys. Lett. **108**, 201902 (2016).
[16] C. Kilic and A. Zunger, Phys. Rev. Lett. **88**, 095501 (2002).
[17] A. Walsh, J. L. F. Da Silva, S.-H. Wei, C. Körber, A. Klein, L. F. J. Piper, A. DeMasi, K. E. Smith, G. Panaccione, P. Torelli, D. J. Payne, A. Bourlange, and R. G. Egdell, Phys. Rev. Lett. **100**, 167402 (2008).
[18] G. Hautier, A. Miglio, G. Ceder, G. M. Rignanese, and X. Gonze, Nat. Commun. **4**, 2292 (2013).
[19] V.-A. Ha, F. Ricci, G.-M. Rignanese, and G. Hautier, J. Mater. Chem. C **5**, 5772 (2017).
[20] M. A. Green, A. Ho-Baillie, and H. J. Snaith, Nat. Photonics **8**, 506 (2014).
[21] W.-J. Yin, J.-H. Yang, J. Kang, Y. Yan, and S.-H. Wei, J. Mater. Chem. A **3**, 8926 (2015).
[22] J. S. Manser, J. A. Christians, and P. V. Kamat, Chem. Rev. **116**, 12956 (2016).
[23] Y. Zhao and K. Zhu, Chem. Soc. Rev. **45**, 655 (2016).
[24] M. V. Kovalenko, L. Protesescu, and M. I. Bodnarchuk, Science **358**, 745 (2017).
[25] T. Leijtens, K. A. Bush, R. Prasanna, and M. D. McGehee, Nat. Energy **3**, 828 (2018).
[26] L. Protesescu, S. Yakunin, M. I. Bodnarchuk, F. Krieg, R. Caputo, C. H. Hendon, R. X. Yang, A. Walsh, and M. V. Kovalenko, Nano Lett. **15**, 3692 (2015).
[27] M. A. Becker, R. Vaxenburg, G. Nedelcu, P. C. Sercel, A. Shabaev, M. J. Mehl, J. G. Michopoulos, S. G. Lambrakos, N. Bernstein, J. L. Lyons, T. Stoferle, R. F. Mahrt, M. V. Kovalenko, D. J. Norris, G. Raino, and A. L. Efros, Nature (London) **553**, 189 (2018).
[28] M. Gong, R. Sakidja, R. Goul, D. Ewing, M. Casper, A. Stramel, A. Elliot, and J. Z. Wu, ACS Nano **13**, 1772 (2019).
[29] G. Kresse and D. Joubert, Phys. Rev. B **59**, 1758 (1999).
[30] J. Heyd, G. E. Scuseria, and M. Ernzerhof, J. Chem. Phys. **118**, 8207 (2003).
[31] G. Kresse and J. Furthmüller, Comput. Mater. Sci. **6**, 15 (1996).
[32] M. Shishkin and G. Kresse, Phys. Rev. B **75**, 235102 (2007).
[33] S.-H. Wei and S. B. Zhang, Phys. Rev. B **66**, 155211 (2002).
[34] S.-H. Wei, Comput. Mater. Sci. **30**, 337 (2004).
[35] I. Chung, J.-H. Song, J. Im, J. Androulakis, C. D. Malliakas, H. Li, A. J. Freeman, J. T. Kenney, and M. G. Kanatzidis, J. Am. Chem. Soc. **134**, 8579 (2012).
[36] R. D. Shannon, Acta Crystallogr., Sect. A: Found. Adv. **32**, 751 (1976).
[37] S. Lany and A. Zunger, Phys. Rev. Lett. **98**, 045501 (2007).
[38] B. Lee, C. C. Stoumpos, N. Zhou, F. Hao, C. Malliakas, C. Y. Yeh, T. J. Marks, M. G. Kanatzidis, and R. P. Chang, J. Am. Chem. Soc. **136**, 15379 (2014).